The Astrophysical Journal, 621:643–650, 2005 March 10

THE MASS FUNCTION OF VOID GALAXIES IN THE SLOAN DIGITAL SKY SURVEY DATA RELEASE 2

David M. Goldberg,[1] Timothy D. Jones,[1] Fiona Hoyle,[1] Randall R. Rojas,[1,2]
Michael S. Vogeley,[1] and Michael R. Blanton[3]
Received 2004 June 23; accepted 2004 November 18

ABSTRACT

We estimate the mass function of void galaxies in the second public data release of the Sloan Digital Sky Survey from a sample of 1000 galaxies with local density contrasts of $\delta_v < -0.6$. The galaxy sample is split into ellipticals and spirals using a color-Sérsic index criterion. We estimate the virial masses of ellipticals using the measured spectral line widths along with the observed size. Projection effects and uncertainties in halo properties make mass estimates of spirals more difficult. We use an inversion of the Tully-Fisher relation to estimate the isothermal rotational velocity and introduce a scaling factor to estimate the halo extent. We then fit the measured mass function against a theoretical Press-Schechter model and find that the distribution of galaxies in voids appears to be nearly unbiased compared to the mass.

Subject headings: cosmology: theory — galaxies: luminosity function, mass function — large-scale structure of universe

1. INTRODUCTION

Regions apparently devoid of galaxies (Kirshner et al. 1981) and clusters (Einasto et al. 1980) were discovered in the early 1980s, and the existence of voids was confirmed by subsequent larger surveys at a variety of wavelengths (de Lapparent et al. 1986; da Costa et al. 1988, 1994; Geller & Huchra 1989; Davis et al. 1982; Maurogordato et al. 1992; see Rood [1988] and references therein for a discussion of the history of void detection and interpretation). Although their relative paucity has meant that void galaxies have largely gone overlooked, they remain one of the best probes of the effect of environment and cosmology on galaxy evolution and are perhaps one of the most intriguing new probes into our understanding of structure formation. Voids have been studied statistically using techniques such as the void probability function (Maurogordato & Lachièze-Rey 1987; Lachièze-Rey et al. 1992; Vogeley et al. 1994; Croton et al. 2004; Hoyle & Vogeley 2004), found using void-finding techniques (Pellegrini et al. 1989; Slezak et al. 1993; El-Ad et al. 1996, 1997; Müller et al. 2000; Plionis & Basilakos 2002; Hoyle & Vogeley 2002; 2004), and studied using semianalytic or *N*-body simulations (Mathis & White 2002; Benson et al. 2003; Gottlöber et al. 2003).

Rojas et al. (2004a [photometric data], 2004b [spectroscopic data]) have considered the properties of galaxies that reside in extremely low-density environments. They (Rojas et al. 2004a) identify a sample of 10^3 void galaxies, i.e., galaxies that are found in regions that have density contrast $\delta_v \equiv \delta\rho/\rho < -0.6$, detected using the Sloan Digital Sky Survey (SDSS; York et al. 2000; Stoughton et al. 2002; Abazajian et al. 2004; Strauss et al. 2004). The properties of galaxies in voids clearly differ from those in higher density regions, as seen in previous studies of void galaxies that include examination of spectral and photometric properties (Moody et al. 1987; Weistrop et al. 1995; Popescu et al. 1997; Grogin & Geller 1999, 2000) and H I content (Szomoru et al. 1996; Huchtmeier et al. 1997). Grogin & Geller (1999, 2000) analyze a sample of 46 galaxies in regions with density less than half of the mean density (i.e., $\delta\rho/\rho < -0.5$) and find that these void galaxies are bluer, of earlier type, and have a larger fraction of emission-line systems than galaxies in dense regions. Similarly, Rojas et al. (2004a) find that void galaxies are bluer, fainter, and have morphologies, as classified by their Sérsic and concentration indices, that more closely resemble late-type galaxies, as compared to galaxies that reside in higher density environments (wall galaxies). Rojas et al. (2004b) also find that void galaxies have stronger equivalent widths of Hα and O II and have higher *specific* star formation rates. Hoyle et al. (2003) measure the luminosity function (LF) of these galaxies and find that the LFs of the wall and void galaxies have different values of M_{r*} (where magnitudes are in SDSS bands unless stated otherwise), i.e., void galaxies are fainter than wall galaxies, but the values of the faint end slopes are very similar: $\alpha = -1.18 \pm 0.13$ and -1.19 ± 0.07, respectively. This suggests that voids are not dominated by a large population of low-luminosity galaxies.

An important question is whether voids are strongly antibiased. Do they contain significant amounts of dark matter, although they are largely devoid of light? We would like to test this question by determining the mass function of void galaxies and estimating their local bias parameter. The bias parameter, b, is defined as the ratio of galaxy perturbations to the perturbations in the underlying dark matter distribution. For an unbiased distribution, $b = 1$, the density contrast of galaxies reflects the density contrast in dark matter.

Void regions also provide an important test bed for the overall picture of galaxy formation because Birkhoff's (1923) theorem suggests that the behavior of structure growth within an underdense or overdense region will mimic that of a universe with the same mean properties. Goldberg & Vogeley (2004) suggest a prescription to efficiently simulate the growth of structure in voids by providing a mapping between the cosmological parameters in the universe as a whole and the effective parameters within the void region. Thus, the formation and evolution of galaxies within voids gives us the opportunity to test the spherical collapse picture of halo formation (Press & Schechter 1974) within highly underdense regions. Sheth & van de Weygaert (2004) explore a second level of excursion when an underdense void is nested within a higher density region.

[1] Department of Physics, Drexel University, 816 Disque Hall, 3141 Chestnut Street, Philadelphia, PA 19104.
[2] Raytheon Corporation, Los Angeles, CA.
[3] Department of Physics, New York University, 4 Washington Place, New York, NY 10003.

In this paper, we measure the void galaxy mass function in the Rojas et al. (2004a) distant galaxy sample, and compare this to theoretical models of void mass functions, in an attempt to understand the environmental effects of low-density regions on galaxy formation. In § 2 we begin by introducing the SDSS void galaxy catalog. Next, in § 3 we discuss mass estimation of the galaxies in this sample. Because the SDSS does not include long-slit spectroscopy, we do not have rotation curves for our sample. Thus, we use an inversion of the Tully-Fisher relation to statistically estimate the rotational velocities of our spiral sample. In § 4 we present a theoretical basis for our expectations of the mass function based on a Press-Schechter model within an underdense region. We then present the comparison of theory with the measured mass function in § 5 and find that "typical" void regions are consistent with an unbiased galaxy formation picture. We conclude with a discussion of future prospects.

2. THE VOID GALAXY CATALOG

To obtain a sample of 10^3 void galaxies, we use data from the Sloan Digital Sky Survey. The SDSS is a wide-field photometric and spectroscopic survey. The completed survey will cover approximately 10^4 deg^2. CCD imaging of 10^8 galaxies in five colors and follow-up spectroscopy of 10^6 galaxies with $r < 17.77$ will be obtained. York et al. (2000) provide an overview of the SDSS, and Stoughton et al. (2002) describe the early data release (EDR) and details about the photometric and spectroscopic measurements. Strauss et al. (2004) describe the second data release (DR2). Technical articles providing details of the SDSS include descriptions of the photometric camera (Gunn et al. 1998), photometric analysis (Lupton et al. 2002), the photometric system (Fukugita et al. 1996; Smith et al. 2002), the photometric monitor (Hogg et al. 2001), astrometric calibration (Pier et al. 2003), selection of the galaxy spectroscopic samples (Strauss et al. 2002; Eisenstein et al. 2001), and spectroscopic tiling (Blanton et al. 2003a). A thorough analysis of possible systematic uncertainties in the galaxy samples is described in Scranton et al. (2002). Galaxy photometry is *k*-corrected and evolution-corrected according to Blanton et al. (2003b). We assume an $\Omega_m = 0.3$, $\Omega_\Lambda = 0.7$ cosmology and Hubble's constant $h = H_0/100$ km s^{-1} Mpc^{-1} throughout.

Void galaxies are drawn from a sample referred to as *sample10* (M. Blanton et al., private communication), which is a subsample of the publicly available DR2. This sample covers nearly 2000 deg^2 and contains 155,126 galaxies. We use a nearest neighbor analysis to find galaxies that reside in regions of density contrast $\delta\rho/\rho < -0.6$ as measured on a scale of 7 h^{-1} Mpc. These are the void galaxies. This choice of density contrast and nomenclature is consistent with studies of voids in more three-dimensional samples, in which individual void structures are identified using an objective *voidfinder* algorithm (Hoyle & Vogeley 2002, 2004). This definition finds voids in the Two-Degree Field Galaxy Redshift Survey (2dFGRS), Point-Source Catalog Redshift Survey (PSCz), and Updated Zwicky Catalog with typical radii of 12.5 h^{-1} Mpc. These voids fill 40% of the universe and have mean density $\delta\rho/\rho < -0.9$. As expected, the density around void galaxies ($\rho_{\rm vg}$) is higher than the mean density of a void ($\bar{\rho}_{\rm void}$) because galaxies are clustered, and the few void galaxies tend to lie close to the edges of the voids. Other techniques, such as the method of El-Ad & Piran (1997), or use of tessellation techniques could also be used to find void galaxies, but currently the geometry of the SDSS does not allow these techniques to be used, as the SDSS is primarily composed of thin stripes, which cannot wholly encompass the largest voids.

The exact process of selecting the void galaxies is described in detail in Rojas et al. (2004a). We provide a brief overview, as follows: first, a volume-limited sample with $z_{\rm max} = 0.089$ is constructed. This is used to trace the distribution of the voids. Any galaxy in the full flux-limited sample with redshift $z < z_{\rm max}$ that has less then three volume-limited neighbors in a sphere with radius 7 h^{-1} Mpc and that does not lie close to the edge of the survey is considered a void galaxy. Galaxies with more than three neighbors are called wall galaxies. Flux-limited galaxies that lie close to the survey boundary are removed from either sample, as it is impossible to tell whether a galaxy is a void galaxy or if its neighbors have not yet been observed. This produces a sample of 1010 void galaxies and 12,732 wall galaxies. These void and wall galaxies have redshifts in the range $0.034 < z < 0.089$ and magnitudes in the range $-22 < M_r < -17$ (Rojas et al. 2004a).

3. MASS ESTIMATION OF GALAXIES

The mass function of galaxies is one of the most sensitive probes of the effect of environment on the growth of structure. The mass function is directly related to the linear growth scale of structure and the power spectrum of the cold dark matter (CDM) distribution. One of the complications in comparing a theoretical mass function to observations is that the simplest theories generally map the mass function of dark matter halos, which are not directly observable. In the following section, we discuss methods for using observations to estimate the halo masses.

3.1. *Classification of Morphologies*

Many properties of galaxies, such as color, luminosity, and rotational velocity vary with morphology. The surface brightness profiles of the different morphological types are found to vary predictably, with spiral types being more compact and ellipticals being more extended. The surface brightness profiles of galaxies are well approximated by the relation

$$I(R) \propto \exp\left[-\left(\frac{R}{R_s}\right)^{1/n}\right], \quad (1)$$

where n is known as the Sérsic (1968) index, such that $n = 1$ for a purely exponential disk, and $n = 4$ for a de Vaucouleurs profile.

Strateva et al. (2001) found a correlation between morphology, color ($g - r$), and concentration. There is a bimodal distribution in color-Sérsic space. M. Blanton et al. (2005, private communication) use $n < 1.5$ as the selection criterion for disk galaxies and $n > 3$ for elliptical galaxies. Rojas et al. (2004a) uses a $n_{\rm crit} = 1.8$ cut to divide their sample between spiral and elliptical types. In this paper, we split the sample in the color-n plane with $n_{\rm crit} = 6[1 - (g - r)]$, as shown in Figure 1. Galaxies whose Sérsic index fall below $n_{\rm crit}$ are classified as spiral, while galaxies whose Sérsic index lie on or are above $n_{\rm crit}$ are classified as elliptical.

In our sample, we found 370 elliptical and 640 spiral galaxies. However, since the sample is flux-limited and not volume-limited, in order to estimate the fraction found in spirals, we must weight by the volume in which each galaxy could be detected. Using this metric, we find that 82% of void galaxies are spirals and 18% are ellipticals. This extends the general morphology-density relation as found, for example, by Postman & Geller (1984).

3.2. *Mass Estimation of Ellipticals*

Elliptical galaxies have a much simpler structure than spirals, thus simplifying the modeling of ellipticals. In this paper,

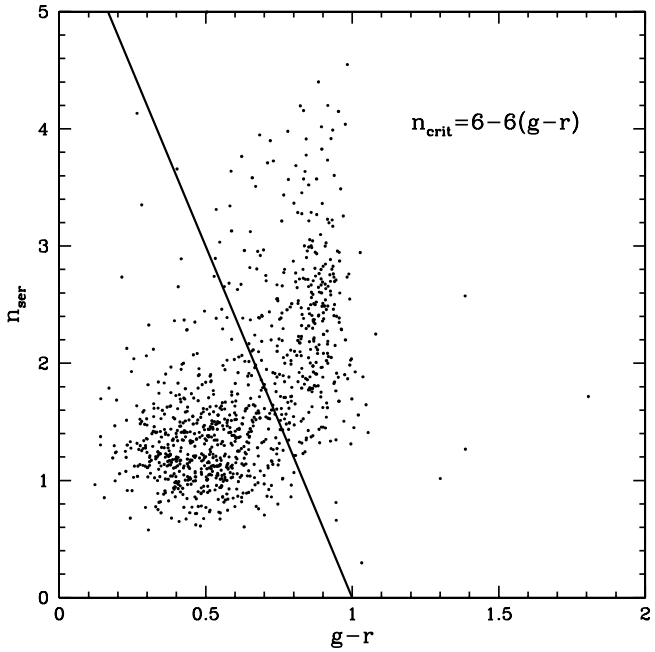

FIG. 1.—Void galaxies in Sérsic index–color space. A partition line of $n_{\rm crit} = 6[1 - (g - r)]$ divides our sample. The galaxies to the right of the partition line are classified as ellipticals, and the galaxies to the left of the partition line are classified as spirals.

we follow Padmanabhan et al. (2004) and fit the circular velocity profile of their model to *N*-body simulations. They find a dynamical mass estimate at R_{50} of

$$M_{\rm dyn,e} = \frac{(1.65\sigma)^2 R_{50}}{G}, \tag{2}$$

where R_{50} is the circular half-light radius of a galaxy, and σ is the one-dimensional velocity dispersion, as defined by the line width of Hα. We use this line both because of its strength and because of its completeness within our sample. The SDSS obtains spectra using a 3″ fiber spectrograph, and thus it is not possible to compute rotation curves or velocity profiles for the galaxy sample. However, Padmanabhan et al. constructed a composite velocity profile for their sample of 29,469 SDSS galaxies and find a nearly isothermal profile for early type galaxies. Thus, the 1_D velocity width directly yields the temperature of the halo, greatly simplifying the dynamical mass estimate of ellipticals.

Equation (2) only gives the mass out to the half-light radius. However, since Padmanabhan et al. (2004) assume that the halo follows a Navarro-Frenk-White (NFW) profile, the integrated mass is, in principle, well defined. Given only a velocity width and an apparent size, however, we have too few parameters to uniquely determine an NFW profile (2 parameters) and a light profile (1 parameter) without implicitly coupling the two. Making an assumption that halo scales with the apparent luminous scale, Figure 10 of Padmanabhan et al. (2004) suggests that a factor of 4 will relate the total mass to that found in equation (2). We use this relation in our analysis below.

3.3. *Mass Estimation of Spirals*

Ideally, we would like to directly measure the dynamical masses of spirals as well as ellipticals. However, the SDSS uses a fiber spectrograph that does not allow us to directly probe the rotation curves of spirals. However, we *can* estimate the rotation velocity via an inversion of the Tully-Fisher (hereafter TF) relation. Courteau (1997) finds a relatively small (∼0.34 mag) scatter in the optical TF relation in the Lick *r* band. In terms of the most relevant measures, Courteau's (1997) TF relation can be expressed as

$$M_c^r = -6.17\left[\log\left(v_{c,2.2}\right) - 2.5\right] - 20.77, \tag{3}$$

where $v_{c,2.2}$ is the rotation radius at 2.2 times the scale length (generally the peak velocity) and M_c^r is the total integrated magnitude in the Lick *r* filter. The intrinsic scatter in the TF relation can be inverted to produce a relatively small scatter in the estimated rotational velocity, such that

$$\frac{\sigma_{v_{c,2.2}^2}}{v_{c,2.2}^2} \simeq 0.26. \tag{4}$$

The Lick *r* filter used by Courteau (1996) was based on the older Lick Spinrad *r* filter. However, Courteau (1996) demonstrates that their photometry is effectively calibrated to the Gunn *r*-system to within 0.01 mag for late-type galaxies. Fukugita et al. (1995) show that at low redshift the magnitude difference between the Gunn *r* filter and the SDSS r' filter is $r' - r = -0.13$, which we adapt to invert the Courteau (1997) TF relation.

Magnitudes are determined in the SDSS data set from Petrosian (1976) radii, defined such that the mean circularly averaged flux within the Petrosian radius is 5 times the flux over the annulus. The SDSS Petrosian magnitude (Blanton et al. 2001) is the measured magnitude within 2 Petrosian radii. For a simple exponential disk model (as is likely to closely approximate the spiral sample), it can be shown that the Petrosian magnitude should be 0.006 higher than a theoretical total magnitude. This effect is significantly smaller than other random and systematic errors that dominate this analysis.

Systematic uncertainty in the overall size of the galactic halos dominates the uncertainty in mass estimates. It is well known that for galaxies the halo extends far beyond the visible limits of the disk. We thus define a dark halo scale factor, *S*, such that:

$$M_{\rm dyn,s} = S\frac{v_{c,2.2}^2 R_{90}}{G}. \tag{5}$$

We have selected R_{90} (the radius containing 90% of the light) to correspond to the visible extent of a disk, and thus we expect that the parameter *S* will necessarily be larger than 1. We can approximate an upper bound on reasonable values for *S* by considering the Milky Way. Given a mass of $M_{\rm MW} \simeq 1.9 \times 10^{12}\ M_\odot$ (Wilkinson & Evans 1999), an isothermal rotational velocity of 220 km s^{-1}, and modeling the light from the Milky Way as a purely exponential disk with a disk scale, $R_d = 2.5$ kpc (Freudenreich 1998), we can estimate a value of R_{90} that would be observed for a given projection angle. Averaging over all angles, we find a limit of about $S = 35$. Environment, however, is expected to strongly affect this scale. In § 5, we show that it is possible to use the dark halo scale factor as a free parameter in our fits, but that high end values (such as that estimated from the Milky Way) give a very poor fit between theory and observation.

We might reasonably wonder if *S* is expected to be a constant function of mass within a given environment. Simple dimensional analysis shows that given a canonical TF relation ($L \propto v^4$), an assumption of constant central flux density, and a constant mass/light ratio, *S* will be constant. In reality, we do not expect this to perfectly model the mass function, and we

thus leave the question of the relation between dark matter extent and mass to future work.

4. PRESS-SCHECHTER MODELS OF GALAXY HALOS IN VOIDS

In § 3, we described our method for determining the mass function of galaxies within cosmological voids. We might also be tempted to ask what mass function we might expect within a void of a particular mean underdensity. This question can be addressed using the Press-Schechter (1974) formalism. We use an approach and notation following that of Mo & White (1996; 2002) but within the context of a constraint on the mean underdensity.

Our approach is quite similar to the work by Gottlöber et al. (2003; following Sheth & Tormen 2002), and for moderate values of the void underdensity, the predicted mass functions are nearly identical. However, there are several key differences. First, Sheth & Tormen frame their discussion in terms of a barrier crossing under Brownian motion. Our formalism is wholly Bayesian. Secondly, the constraint placed by Gottlöber et al. is based on a polynomial fit to the growth of an underdense perturbation. We base our prior on a numerical approach described in Goldberg & Vogeley (2004). Gottlöber et al. also note that, following Birkhoff's theorem, the interior of the void may be treated as an isolated universe with mean density given by the void density. However, unlike Goldberg & Vogeley (2004), they do not correct the critical density of the void (and thus the interior value of Ω) to reflect the fact that the voids expand faster than the background universe, and thus have a higher local value of the Hubble constant. Finally, the formalism allows an explicit dependence on the scale of the void. Despite these differences, even a in highly underdense region, $\delta_v \simeq -0.8$, the results presented below are consistent with those of Gottlöber et al. to within about 20% up to masses of $10^{11}\ M_\odot$. Furthermore, as shown in Goldberg & Vogeley (2004), both estimates produce a satisfactory agreement in mass function with both large-scale simulation and the "bottle universe" simulations described in the same paper.

4.1. *Calculation of the Mass Function*

Consider a Gaussian random field of density perturbations, $\delta(\boldsymbol{r})$, on which we apply an isotropic smoothing filter of characteristic scale, R, $W(r;\ R)$, such that we have a smoothed density field

$$\delta(\boldsymbol{r};\ R) \equiv \int W(|\boldsymbol{r}-\boldsymbol{r}'|;\ R)\delta(\boldsymbol{r}')\, d^3\boldsymbol{r}'. \tag{6}$$

As the new field is simply a linear sum of the underlying field, the distribution of the smoothed field is also a Gaussian with mean zero and a variance of

$$\Delta^2(R) \equiv \left\langle \delta(\boldsymbol{r};\ R)^2 \right\rangle = \int P(k)\left|\hat{W}(k;\ R)\right|^2 d^3\boldsymbol{k}, \tag{7}$$

where $\hat{W}(k;\ R)$ is the Fourier transform of the smoothing kernel, and $P(k)$ is the power spectrum of perturbations of the underlying field,

$$P(k) = \left\langle \left|\hat{\delta}^2_{\boldsymbol{k}}\right| \right\rangle, \tag{8}$$

which is assumed to be isotropic.

Now let us further consider the covariance of a field that is smoothed on two different scales:

$$V_{12} \equiv \langle \delta(\boldsymbol{r};\ R_1)\delta(\boldsymbol{r};\ R_2)\rangle = \int P(k)\hat{W}(k;\ R_1)\hat{W}*(k;\ R_2)\, d^3\boldsymbol{k}. \tag{9}$$

Since the real-space window functions are spherically symmetric, the Fourier space convolutions over the window functions on the void and perturbation scale produce a real covariance.

Let us now consider a density perturbation, δ, on a scale, R, in which all un-subscripted variables (R, M, δ) are assumed to be at the current epoch. This perturbation arises in a larger region, R_v, which has a mean *linear* underdensity, δ_v^L.

We might imagine that at early times, a highly underdense void satisfied the relationship, $\delta^L_{v,z}/D(z) < -1$. In other words, we would naively expect it to evolve to negative density today. This is a natural limitation on linear theory, and, thus, we define δ_v as the underdensity that the void *would* have were it allowed to linearly evolve indefinitely, a value that can be less than -1. Goldberg & Vogeley (2004) derive an integral form for this expression and relate it to a simple parameter, η, such that

$$\delta_v^L = \eta(\delta_v,\ \Omega_M,\ \Omega_\Lambda)\delta_0(\Omega_M,\ \Omega_\Lambda), \tag{10}$$

where δ_v is the "true" underdensity of the void at the present epoch, $\delta_v^L \leq \delta_v$, Ω_M is the matter density relative to critical, Ω_Λ is the cosmological constant density relative to critical, and δ_0 is the relative structure growth factor as defined in Carroll et al. (1992).

The joint probability density of finding a field with density δ on scale R and within a region of mean density δ_v^L on scale R_v is thus a bivariate Gaussian with a covariance matrix

$$V = \begin{pmatrix} \Delta^2 & V_{0v} \\ V_{0v} & \Delta_v^2 \end{pmatrix}, \tag{11}$$

where all terms in the covariance matrix are defined as parameters at the present epoch. However, since all perturbations are expected to grow as $D(z)$, this relation can be readily modified [via a substitution of $\delta_z = D(z)\delta$ and so on] at all times.

It can thus be shown that for a bivariate Gaussian with the covariance matrix as above,

$$f\left(\delta; R|\delta_v^L; R_v\right) = \mathcal{N}\left(\delta_v \frac{V_{0v}}{\Delta_v^2},\ \sqrt{\Delta^2 - \frac{V_{0v}^2}{\Delta_v^2}}\right) \tag{12}$$

$$\equiv \mathcal{N}(\mu(R),\ \sigma(R)), \tag{13}$$

where $\mathcal{N}(\mu, \sigma)$ represents the normalized Gaussian distribution function. For brevity, we will henceforth not explicitly state the prior condition δ_v^L, R_v.

Defining

$$x \equiv \frac{\delta - \mu}{\sigma}, \tag{14}$$

equation (13) simply becomes $f(x) = \mathcal{N}(0, 1)$.

A principal result of the spherical collapse model (Press & Schechter 1974; Peebles 1980) is that (in an $\Omega_M = 1$ universe) any region for which the smoothed density is greater than $\delta_c > 1.69$ has reached a maximum expansion in the linear

approximation and has begun to collapse. However, this critical overdensity is similar in most cosmologies.

Bond et al. (1991) show that the cumulative probability of finding a collapsing/collapsed mass exceeding M at redshift z is thus

$$F(M, z) = \mathrm{erfc}\left(\frac{\nu}{\sqrt{2}}\right), \tag{15}$$

where the factor of 2 in front stems from normalization of the mass distribution. Note that R and M are equivalent measures of a perturbation, such that

$$M = \frac{4\pi}{3}\rho_0 R^3, \tag{16}$$

where ρ_0 is the mean density of the universe at present. Finally,

$$\nu \equiv \frac{\delta_c/D(z) - \mu}{\sigma}. \tag{17}$$

Relating the perturbation distribution to a mass function, we get

$$\begin{aligned} n(M, z)\,dM &= -\frac{dF}{dM}\frac{\rho_0}{M}(1+\delta_{v,z})\,dM \\ &= \sqrt{\frac{2}{\pi}}\exp\left(-\frac{\nu^2}{2}\right)(1+\delta_{v,z})\frac{\rho_0}{M}\frac{d\nu}{dM}\,dM, \end{aligned} \tag{18}$$

where the $1+\delta_{v,z}$ term normalizes the commoving volume (set by the background universe) to the physical volume at any given time, and ν is implicitly a function of redshift.

This model was derived using spherical collapse approximations. However, following Sheth et al. (2001), we can incorporate an elliptical collapse model:

$$\begin{aligned} n(M, z)\,dM = A\left(1+\frac{1}{\nu'^{2q}}\right)\sqrt{\frac{2}{\pi}}\exp\left(-\frac{\nu'^2}{2}\right) \\ \times (1+\delta_{v,z})\frac{\rho_0}{M}\frac{d\nu'}{dM}\,dM, \end{aligned} \tag{19}$$

where $\nu' = \sqrt{a}\nu$, $a = 0.707$, $A = 0.322$, and $q = 0.3$. Simulations (e.g., Jenkins et al. 2001) suggest that the ellipsoid model produces a good fit to galaxy abundances. We use the ellipsoidal distribution function throughout the forgoing analysis.

4.2. *The Growth of Galaxies in Voids*

Before moving on to the observed mass function and a comparison with theory, we discuss briefly the implications of the growth of void galaxies in the model above. It is clear that with less matter available to grow galaxies, void regions must necessarily contain far fewer of them. Indeed, this is how voids are identified. Moreover, if we were to identify perturbations of equal amplitude at early times in a void and in the background, the background perturbation would grow into a visible galaxy faster and would have a much larger final mass than the void galaxy.

However, we wish to ask the converse: given an observed void galaxy or galaxy distribution *today*, what is a likely formation history? Goldberg & Vogeley (2004) discuss the evolution of the linear growth parameter, $D(z)$, in some detail. As

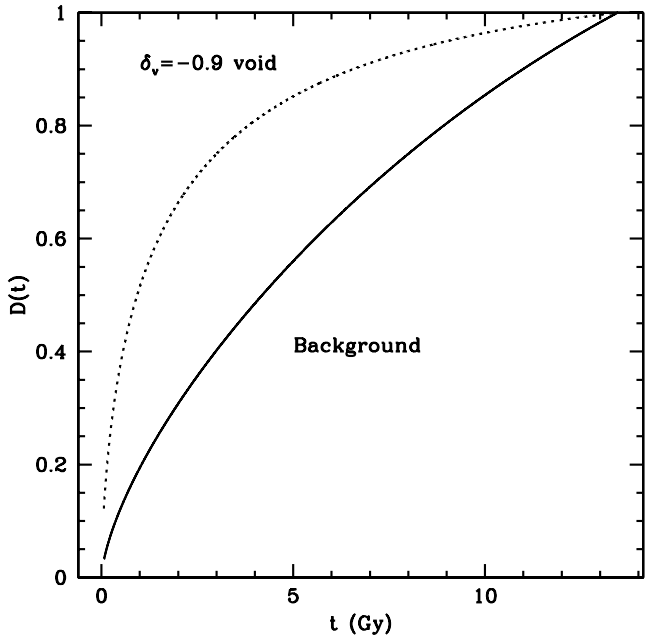

FIG. 2.—Normalized linear growth parameter within a background $\Omega_M = 0.3$ flat cosmology and within a $\delta_v = -0.9$ void. Note that the void growth parameter achieves a higher fraction of the present value in the void than in the background for all points in the past.

Figure 2 illustrates, the growth parameter achieves a higher fraction of its present value at early times in voids than in the background universe. This argument is similar to the ones accompanying the normalization of σ_8 in open versus flat cosmologies, stemming from the well-known result that perturbations "freeze out" at $z \simeq \Omega_M^{-1} - 1$ in low-density universes. In other words, we would expect that, given two galaxies of equal mass, one identified in the field, and one in a void, the void galaxy would have been more fully formed (in terms of its present mass) at earlier times.

Another way of looking at this is in terms of the evolution of the mass function. In Figure 3 we show the time dependence of the $M > 10^{10}$ and $M > 10^{12}\ h^{-1}\ M_\odot$ slice through the mass function both in voids (*dotted lines*) and in the background cosmology (*solid lines*). We do not use the $1+\delta_v$ volume correction, so that at each epoch we have the same commoving volume. At first glance, Figure 3 gives an interpretation of structure growth that is the opposite of what we conclude from Figure 2. For both intermediate- and high-mass galaxies, we find a larger fractional increase in the number density at recent epochs in void regions than in the background. This effect happens because the mass function is much steeper at high masses for voids than for the background. As a result, a small growth in structure results in the production of (fractionally) many more galaxies at high masses.

Finally, we can ask, how much matter has any *given* galaxy accreted since a previous epoch? We may set a density threshold and ask, for a given epoch, for what mass is the cumulative mass function equal to that density? The bottom panels in Figure 3 show the evolution of this function for 10^{10} (*left*) and 10^{12} (*right*) $h^{-1}\ M_\odot$. The fact that in the background a $10^{10}\ h^{-1}\ M_\odot$ galaxy achieves a maximum mass around $z \simeq 1.5$ suggests that a significant fraction of this mass accretion is in the form of mergers. This simple picture suggests that for the few high-mass galaxies in voids, we would expect a relatively high fraction of recent mass accretion. This is consistent with the result found by Rojas

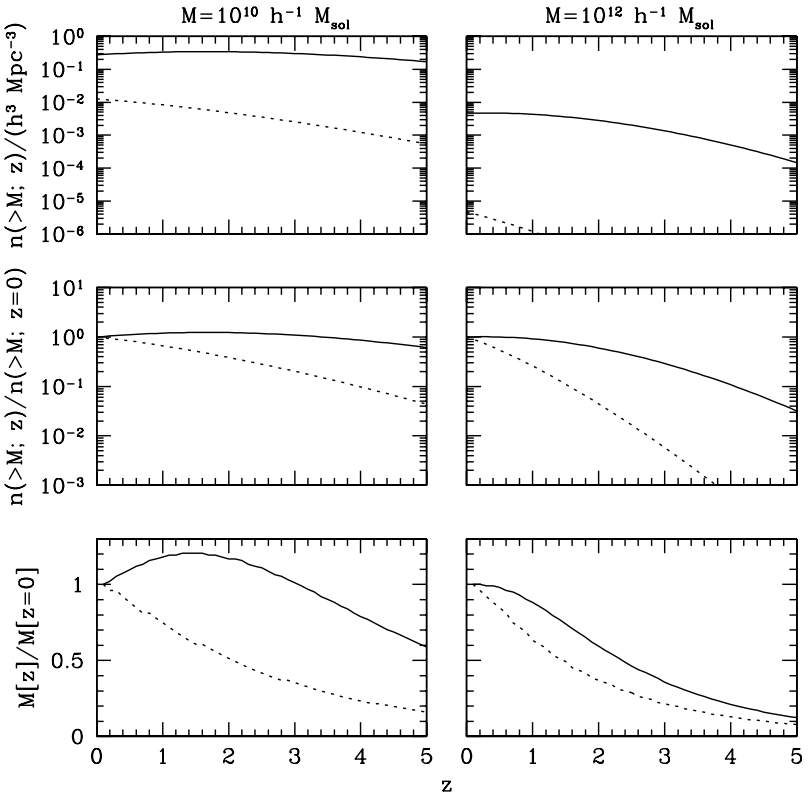

FIG. 3.—Evolution of a theoretical galaxy mass function in a $\delta_v = -0.9$ void (*dotted lines*) and in the background (*solid lines*). For each, we compute the evolution of the $N(>10^{10}\ h^{-1}\ M_\odot)$ (*left*) and $N(>10^{12}\ h^{-1}\ M_\odot)$ (*right*) distribution. The top set of panels shows the evolution of the cumulative mass function for each fiducial mass. These are normalized to commoving volume. The middle panels show the mass function normalized to the present. The bottom panels show the evolution of a halo mass (described in the text) of 10^{10} and $10^{12}\ h^{-1}\ M_\odot$ galaxies at earlier epochs.

et al. (2004b), who found a relatively high specific star formation rate in voids compared to wall regions.

5. RESULTS: THE VOID MASS FUNCTION IN THE SDSS

In Figure 4, we show the estimated SDSS void galaxy mass function for dark matter scale factors $S = 2$, 5, and 10. For comparison, we also show the expected Press-Schechter mass functions for $\delta_v = -0.9$ (observed mean galaxy underdensity) and $\delta_v = 0$ (background) environments and determine the best value of δ_v for each value of S by matching the cumulative number density of objects at 4 times the mass detection limit.

We note that the minimum value of R_{90} observed in the spiral sample is approximately 2 kpc, and that the maximum observable absolute magnitude is -18. Combining these results, we find a minimum detectable mass of $S \times 6 \times 10^9\ h^{-1}\ M_\odot$. This mass detection limit is shown by a vertical dashed line in the bottom panels of Figure 4. The mass detection limit is determined by relating the flux-limited minimum velocity estimate with a fit relation between size and luminosity. It should be noted that the mass function does not flatten out considerably beyond this limit. In other words, we do not see a deficit of low-mass/low-luminosity galaxies in voids beyond what is expected by Press-Schechter analysis and our detection limit. In addition to plotting the mass function for all galaxies, we subdivide our sample into ellipticals and spirals in Figure 4. Ellipticals clearly constitute the high-mass end of the spectrum, and their distribution tends to be much flatter than the distribution of spirals, which dominate at low and intermediate mass.

For comparison, we plot a mass function estimated from the stellar mass distribution given by Kauffmann et al. (2003) from the SDSS First Data Release (Abazajian et al. 2004). To turn these into total mass distributions, we assume a constant mass–stellar mass ratio of 3, as estimated for ellipticals by Padmanabhan et al. 2004. The mass–stellar mass ratio of spirals is expected to be larger than for ellipticals, even if the baryon ratio for both is the same, since spirals are expected to be more gas rich. It is clear, however, that this simple estimate of the mass function does not produce a good fit to the slope of the Press-Schechter mass functions.

For our "dynamical" mass estimates, lower values of S appear to produce a better fit to the shape of a Press-Schechter mass function. This is confirmed via a series of χ^2 tests. For $S = 2$, 5, and 10, the fits to $\delta_v = -0.82$, -0.73, and -0.62, respectively, produce χ^2 per degree of freedom of 3.3, 8.2, and 14.7. Note that we only model this fit out to masses of $5 \times 10^{12}\ M_\odot$. Beyond that, all three models produce at most one galaxy per bin, in each case an elliptical. Since these galaxy masses are somewhat unreasonably large, it may be that we have simply underestimated the uncertainty in velocity measurement for the Ellipticals.

Since in all cases we measure $\chi^2 > 1$, it is clear that despite an excellent "chi-by-eye," we have not correctly characterized either our uncertainties or our mass measurements. One of the most likely culprits is that the halo extent parameter, S, is an explicit function of mass. Given the other uncertainties in our measurements, it is unrealistically optimistic to try to claim a functional form of this term with any confidence.

Since a given value of S implies an underdensity in dark matter for the ensemble of voids, we show, in Figure 5, the explicit relationship between these two terms. Moreover, a simple

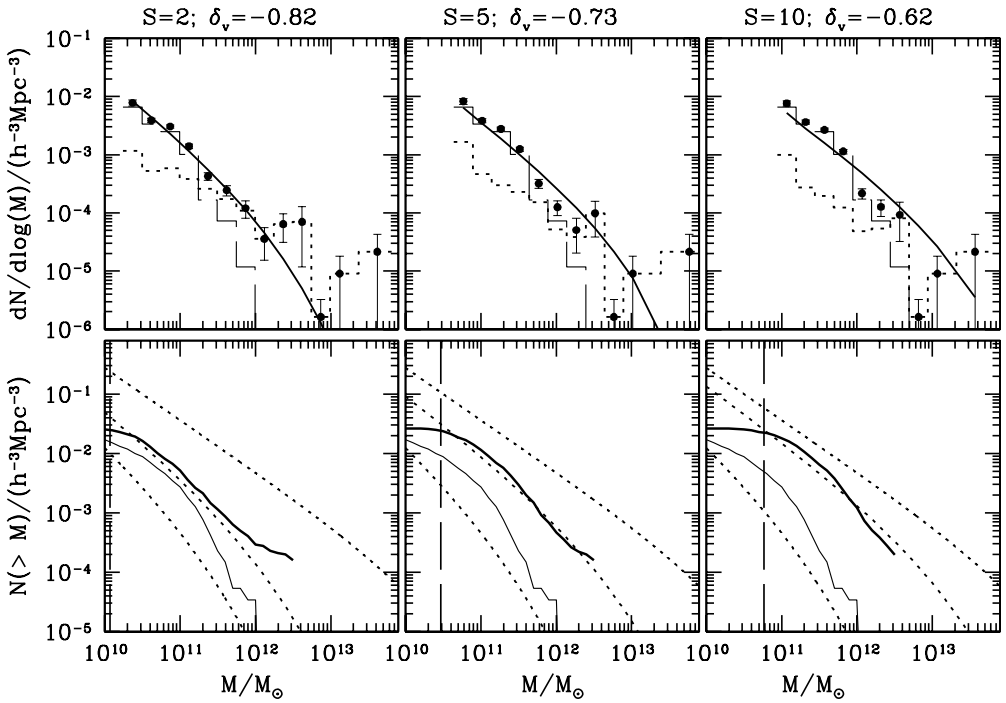

FIG. 4.—Comparison between theoretical and estimated dynamical mass functions of the void galaxies in the SDSS Data Release 2. In each, we vary the dark halo scale factor, S, such that $S = 2, 5$, and 10 (*from left to right*). *Top panels*: Differential mass functions, with error bars within bins given by Poisson errors. Random errors of 26% in v^2 are applied by convolving (flattening) the model distribution function. The solid line represents the best-fit DM halo model of $\delta_v = \{-0.82, -0.73, -0.62\}$. No errors are given for the (unknown) systematic uncertainties arising from the halo extent. In each, the long-dashed histogram shows the distribution of spirals, and the short-dashed histogram shows the distribution of ellipticals. *Bottom panels*: Cumulative mass functions. The vertical line represents the mass detection limit for each assumed scale factor. The bold line represents the measured dynamical mass function. The thin line represents the mass function obtained from an assumed mass–stellar mass ratio of 3 from the stellar mass estimates of Kauffmann et al. Note that the inferred masses of ellipticals are the same in all three panels, and only the spiral mass estimates vary with S. Dotted lines show analytic DM mass functions for $\delta_v = -0.9$ (*bottom*), $\delta_v = \{-0.82, -0.73, -0.62\}$ (*middle*), and $\delta_v = 0$ (*top*).

calculation of the "typical" galaxy density within our selected void sample (number of observed galaxies divided by total void volume) yields $\delta_{v,\mathrm{gal}} = -0.77$. Since lower values of S are generally preferred (from a χ^2 point of view), we find that voids may, in fact, be nearly unbiased tracers of dark matter. Even for larger values of $S = 10$, we find $b = 1.24$, consistent with typical bias relations found in the universe at large.

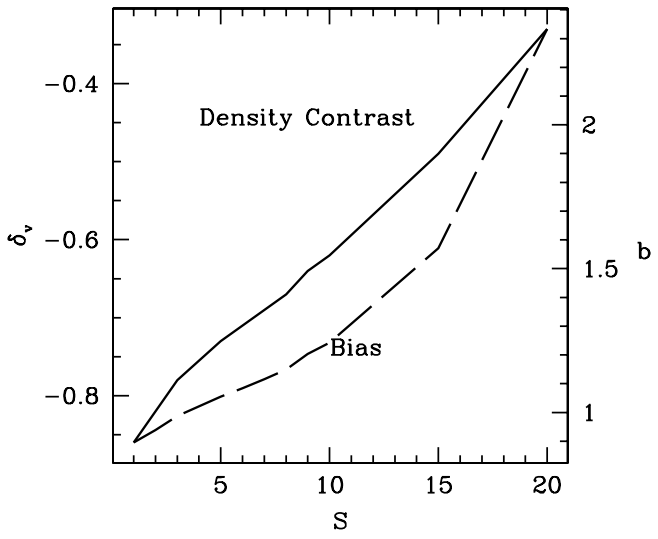

FIG. 5.—Relationship between best-fit density contrast and halo extent parameter. Note that for relatively compact halos (relative to the luminous distribution) we find a fairly unbiased distribution for low values of S and an only modestly (positively) biased distribution for larger values of S.

6. DISCUSSION

There remain several untested assumptions in this study. For example, although compact halos are most consistent with our theoretical mass function models, Press-Schechter has not been tested against observations in very low density void regions. Moreover, we assumed that the TF relation in the field would necessarily hold for void galaxies as well. However, as Rojas et al. (2004a) has shown, the photometric properties of void galaxies differ from those of wall galaxies, and thus we would not be surprised to find a different TF relation.

Future prospects for work in this direction include more systematic estimates of the rotation curves of void spirals. Ideally, follow-up observations using long-slit spectroscopy could potentially yield a TF relation for voids that differs significantly from wall regions.

In addition, as the numbers of known void galaxies increase, galaxy-galaxy gravitational lensing will become a potentially powerful probe for measuring mass profiles and halo extents. Since the separation between a lens and a source galaxy is much larger than the scale of a void ($\Delta z \simeq 0.5$ in many cases), an isolated void galaxy lens may still have many potential sources to lens.

D. M. G. acknowledges support from NSF grant AST 02-05080. M. S. V. acknowledges support from NSF grant AST 00-71201. We thank Michael Strauss for useful suggestions.

REFERENCES

Abazajian, K., et al. 2004, AJ, 128, 502
Benson, A. J., Hoyle, F., Torres, F., & Vogeley, M. S. 2003, MNRAS, 340, 160
Birkhoff, G. D. 1923, Relativity and Modern Physics (Cambridge: Harvard Univ. Press)
Blanton, M. R., et al. 2001, AJ, 121, 2358
———. 2003a, AJ, 125, 2276
———. 2003b, AJ, 125, 2348
Bond, J. R., Cole, S., Efstathiou, G., & Kaiser, N. 1991, ApJ, 379, 440
Carroll, S. M., Press, W. H., & Turner, E. L. 1992, ARA&A, 30, 499
Courteau, S. 1996, ApJS, 103, 363
———. 1997, AJ, 114, 2402
Croton, D. J., et al. 2004, MNRAS, 352, 828
da Costa, L. N., et al. 1988, ApJ, 327, 544
———. 1994, ApJ, 424, L1
Davis, M., Huchra, J. P., Latham, D. W., & Tonry, J. 1982, ApJ, 253, 423
de Lapparent, V., Geller, M. J., & Huchra, J. P. 1986, ApJ, 302, L1
Einasto, J., Joeveer, M., & Saar, E. 1980, MNRAS, 193, 353
Eisenstein, D. J., et al. 2001, AJ, 122, 2267
El-Ad, H., & Piran, T. 1997, ApJ, 491, 421
El-Ad, H., Piran, T., & da Costa, L. N. 1996, ApJ, 462, L13
———. 1997, MNRAS, 287, 790
Freudenreich, H. T. 1998, ApJ, 492, 495
Fukugita, M., Ichikawa, T., Gunn, J. E., Doi, M., Shimasaku, K., & Schneider, D. P. 1996, AJ, 111, 1748
Fukugita, M., Shimasaku, K., & Ichikawa, T. 1995, PASP, 107, 945
Geller, M. J., & Huchra, J. P. 1989, Science, 246, 897
Goldberg, D. M., & Vogeley, M. S. 2004, ApJ, 605, 1
Gottlöber, S., Łokas, E. L., Klypin, A., & Hoffman, Y. 2003, MNRAS, 344, 715
Grogin, N., & Geller, M. J. 1999, AJ, 118, 2561
———. 2000, AJ, 119, 32
Gunn, J. E., et al. 1998, AJ, 116, 3040
Hogg, D. W., Finkbeiner, D. P., Schlegel, D. J., & Gunn, J. E. 2001, AJ, 122, 2129
Hoyle, F., Rojas, R., Vogeley, M. S., & Brinkmann, J. 2003, ApJ, submitted
Hoyle, F., & Vogeley, M. S. 2002, ApJ, 566, 641
———. 2004, ApJ, 607, 751
Huchtmeier, W. K., Hopp, U., & Kuhn, B. 1997, A&A, 319, 67
Jenkins, A., et al. 2001, MNRAS, 321, 372
Kauffmann, G., et al. 2003, MNRAS, 341, 54
Kirshner, R. P., Oemler, A., Jr., Schechter, P. L., & Shectman, S. A. 1981, ApJ, 248, L57
Lachièze-Rey, M., da Costa, L. N., & Maurogordato, S. 1992, ApJ, 399, 10
Lupton, R. H., Ivezic, Z., Gunn, J. E., Knapp, G., Strauss, M., & Yasuda, N. 2002, Proc. SPIE, 4836, 350
Mathis, H., & White, S. D. M. 2002, MNRAS, 337, 1193
Maurogordato, S., & Lachièze-Rey, M. 1987, ApJ, 320, 13
Maurogordato, S., Schaeffer, R., & da Costa, L. N. 1992, ApJ, 390, 17
Mo, H. J., & White, S. D. M. 1996, MNRAS, 282, 347
———. 2002, MNRAS, 336, 112
Moody, J. W., Kirshner, R. P., MacAlpine, G. M., & Gregory, S. A. 1987, ApJ, 314, L33
Müller, V., Arabi-Bidgoli, S., Einasto, J., & Tucker, D. 2000, MNRAS, 318, 280
Padmanabhan, N., et al. 2004, NewA, 9, 329
Peebles, P. J. E. 1980, The Large-Scale Structure of the Universe (Princeton: Princeton Univ. Press)
Pellegrini, P. S., da Costa, L. N., & de Carvalho, R. R. 1989, ApJ, 339, 595
Petrosian, V. 1976, ApJ, 209, L1
Pier, J., et al. 2003, AJ, 125, 1559
Plionis, M., & Basilakos, S. 2002, MNRAS, 330, 399
Popescu, C., Hopp, U., & Elsässer, H. 1997, A&A, 325, 881
Postman, M., & Geller, M. J. 1984, ApJ, 281, 95
Press, W. H., & Schechter, P. 1974, ApJ, 187, 425
Rojas, R., Vogeley, M. S., Hoyle, F., & Brinkmann, J. 2004a, ApJ, 617, 50
———. 2004b, ApJ, submitted (astro-ph/0409074)
Rood, H. J. 1988, ARA&A, 26, 245
Scranton, R., et al. 2002, ApJ, 579, 48
Sérsic, J. L. 1968, Atlas de Galaxias Australes (Cordoba: Observatorio Astronómico)
Sheth, R. K., Mo, H. J., & Tormen, G. 2001, MNRAS, 323, 1
Sheth, R. K., & Tormen, G. 2002, MNRAS, 329, 61
Sheth, R. K., & van de Weygaert, R. 2004, MNRAS, 350, 517
Slezak, E., de Lapparent, V., & Bijaoui, A. 1993, ApJ, 409, 517
Smith, J. A., et al. 2002, AJ, 123, 2121
Stoughton, C., et al. 2002, AJ, 123, 485
Strateva, I., et al. 2001, AJ, 122, 1861
Strauss, M., et al. 2002, AJ, 124, 1810
———. 2004, AJ, 128, 2004
Szomoru, A., van Gorkom, J. H., Gregg, M. D., & Strauss, M. A. 1996, AJ, 111, 2150
Vogeley, M. S., Geller, M. J., Park, C., & Huchra, J. P. 1994, AJ, 108, 745
Weistrop, D., Hintzen, P., Liu, C., Lowenthal, J., Cheng, K. P., Oliversen, R., Brown, L., & Woodgate, B. 1995, AJ, 109, 981
Wilkinson, M. I., & Evans, N. W. 1999, MNRAS, 310, 645
York, D. G., et al. 2000, AJ, 120, 1579